Self-Assembled Micro-Honeycomb Network of Single-Walled Carbon Nanotubes for Solar Cells

Kehang Cui, [1] Takaaki Chiba, [1] Shuichiro Omiya, [1] Theerapol Thurakitseree, [1] Pei Zhao, [1] Shunjiro Fujii,[2] Hiromichi Kataura,[2]Erik Einarsson, [1] Shohei Chiashi, [1] Shigeo Maruyama[1]*

[1]Department of Mechanical Engineering, The University of Tokyo, 7-3-1 Hongo, Bunkyo-ku, Tokyo, 113-8656, Japan

[2] Nanosystem Research Institute, National Institute of Advanced Industrial Science and Technology, 1-1-1 Higashi, Tsukuba 305-8562, Japan

Corresponding Author:

Shigeo Maruyama, maruyama@photon.t.u-tokyo.ac.jp,
Department of Mechanical Engineering, The University of Tokyo, 7-3-1 Hongo, Tokyo, 113-8656, Japan; Tel: +81-3-5841-6421; Fax: +81-3-5800-6983.

ABSTRACT

We propose a water vapor treatment to direct the formation of single-walled carbon nanotubes (SWNTs) into a self-assembled micro-honeycomb network (μ-HN) for the application to SWNT-Si solar cells. The μ-HN consists of vertical aggregated SWNT walls and a buckypaper bottom. This hierarchical structure exhibits lower sheet resistance and higher optical transmittance compared with buckypaper. The pristine μ-HN SWNT-Si solar cell shows a record-high fill factor of 72% as well as a power conversion efficiency (PCE) of 6% without optimizing the diameter or height of the vertically aligned SWNTs. The PCE remains stable for weeks in ambient condition, and a PCE exceeding 10% is achieved in the dry state after dilute nitric acid treatment.
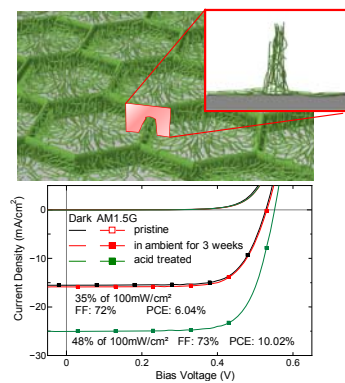
KEYWORDS: Single-walled carbon nanotube, nanotube-Si solar cell, self-assembled, micro-honeycomb network, water vapor treatment

Single-walled carbon nanotubes (SWNTs) feature outstanding electronic, optical, mechanical and thermal properties and hence are considered as one of most promising materials for next-generation optical and electronic devices.[1-3] Indeed, SWNTs have been exploited for photovoltaic and photoelectrochemical cells encompassing all aspects,[4-17] *e.g.* photocurrent generation sites,[4,5] scaffolds[6,7] or electrodes[8,9]. Currently, SWNT-Si solar cells[10-17] with high power-conversion efficiency (PCE) have emergent technological impact. Randomly oriented SWNT films (so-called "buckypaper") are most intensively investigated for this kind of solar cells[10-16]. Efforts in improving the properties of randomly oriented SWNT films have improved the PCE and the fill factor (FF) substantially. However, these improvements have been realized by chemical modification of the random carbon nanotube films, which results in poor stability. In fact, the gap between the superior nanoscale properties of individual SWNTs and the less impressive performance of their micro/macroscale assembly is hindering the realization of their full potential. Carefully designed morphology of SWNTs provides an alternative to efficiently organize the charge generation, separation and transport at solar-cell interfaces.

Self-assembly is a high-yield and low-cost method that builds low-dimensional materials into three-dimensional micro/macro-architectures with various morphologies. Capillary forces have been used to direct the self-assembling of patterned arrays of nanowires,[18] nanopillars[19] and multi-walled carbon nanotubes[20-24] (MWNTs) into hierarchical networks. However, due to the hydrophobicity and significantly smaller diameter of SWNTs, wetting vertically aligned SWNTs (VA-SWNTs) results in a high-density bulk with millimeter-scale cracks[25] rather than the hierarchical honeycomb-like network formed by MWNT arrays. So far, such a honeycomb structure of SWNTs has been achieved only by film-casting anionic shortened SWNTs–cationic ammonium lipid conjugates in organic solution,[26,27] of which the complicated solution preparation induces defects and degradation of SWNTs.

In this letter, we present a novel water vapor treatment process to build up SWNTs to a self-assembled hierarchical micro-honeycomb network (μ-HN) for SWNT/Si solar cell applications. The μ-HN film shows lower sheet resistance and higher optical transmittance compared with collapsed honeycomb network (HN), of which the morphology is close to buckypapers.[28] A stable FF of 72% is achieved for pristine SWNTs with μ-HN, which is the highest FF reported to date for SWNT-Si solar cells. The short circuit current density (J_{sc}) and open circuit voltage (V_{oc}) are 15.9 mA/cm^2 and 530 mV, respectively. The conversion efficiency (PCE) is 6% even after three weeks in air. A PCE exceeding 10% was obtained in the dry state after treatment with dilute nitric acid.

VA-SWNTs were synthesized on Co/Mo dip-coated Si/SiO$_2$ substrates using our conventional alcohol catalytic chemical vapor deposition (ACCVD) process.[29,30] The high G/D ratio obtained by Raman spectroscopy (See Supporting Information S1) demonstrates the good quality of the SWNTs. The average diameter of the SWNTs is approximately 2 nm and the film thickness of the VA-SWNT is 5 ± 0.2 μm. After ACCVD synthesis, the water vapor treatment (Figure 1a) includes two steps: (1) expose the VA-SWNT array to vapor from a hot water reservoir, and (2) turn the substrate over and dry the array in the ambient environment. The uniform VA-SWNT array (Figure 1b) was aggregated into hexagonal frames (intermediate stage shown in Figure 1c), after the first water vapor treatment. By repeating this treatment the VA-SWNT array evolved into a μ-HN (Figure 1d) after 20 to 30 iterations. The liquid-solid interaction induced by the condensation and subsequent evaporation of water is the building tool used to engineer the morphology of VA-SWNTs into a self-assembled μ-HN. The μ-HN is a hierarchical hexagonal-shaped three-dimensional network (Figure 2a) that consists of vertical SWNT walls and a randomly networked SWNT bottom. Each wall is a cross-linked high-density SWNT

agglomeration (Figure 2b) and the bottom of each honeycomb cell is a randomly oriented buckypaper, which results from the collapse of SWNT alignment. The schematic of μ-HN is shown in Figure 2c. The most energetically favorable outcome is a honeycomb network because it uniformly divides the region into cells having minimal perimeter, *i.e.*, allows the largest number of SWNTs to collapse.
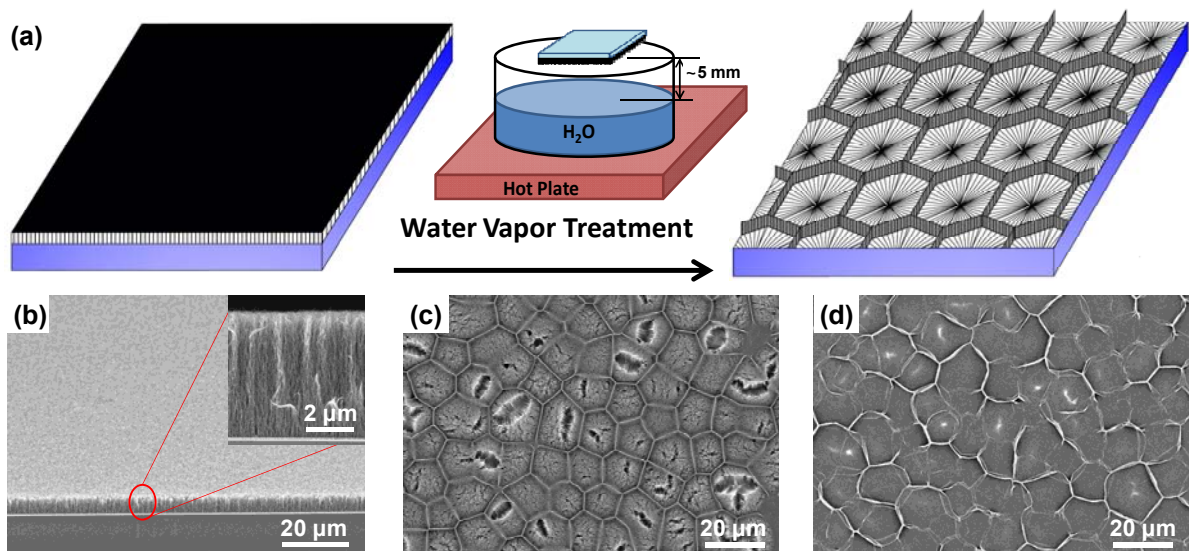

Figure 1. Water vapor treatment of the VA-SWNT array into a μ-HN. (a) Schematic of the water vapor treatment process. (b) As-synthesized high-quality VA-SWNT with a uniform top surface. (c) Intermediate stage of the μ-HN formation after the first iteration. (d) Stable μ-HN formed after 30 times iterations of the water vapor treatment.
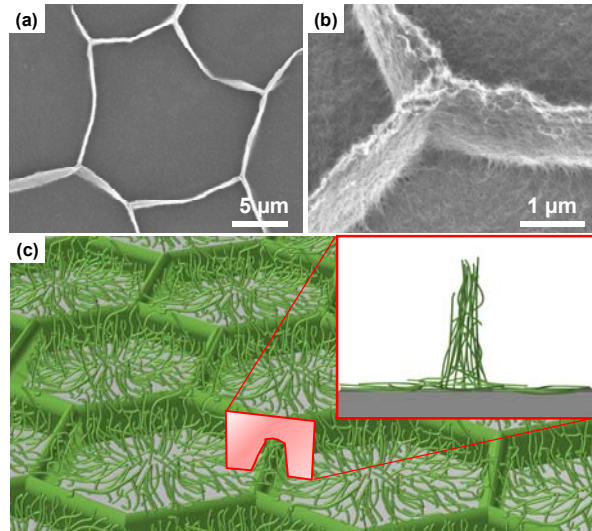
Figure 2. (a) An individual honeycomb cell. (b) Magnified image of the hierarchical structure of μ-HN. The walls are a cross-linked highly-condensed SWNT agglomeration. The bottom of each honeycomb cell is a randomly oriented buckypaper. (c) Schematic of the μ-HN. The inset shows the hierarchical assembly of the μ-HN.

Varying the water reservoir temperature and vapor exposure time of water vapor treatment results in different morphologies. In this letter, three different self-assembled SWNT structures – μ-HN, collapsed HN and porous HN, as shown in Figures 3a-c respectively – are employed for fabricating SWNT-Si solar cells. The μ-HN (Figure 3a) is obtained by the exposure to vapor from an 80 ˚C reservoir for 5 s. Extending the exposure time from 5 s to 15 s at the same reservoir temperature would result in the collapse of the walls, hence larger cell sizes. When the exposure time is more than 15 s, nearly all the wall structures disappear and the whole film becomes a collapsed HN (Figure 3b). The porous HN (Figure 3c) is obtained from 5 s vapor exposure to a water reservoir at 70 ˚C. The detailed parametric investigation on the self-assembly process is described in the Supporting Information S2.

The self-assembled SWNT films can be transferred onto arbitrary substrates by the hot-water thermocapillary method.[31] The SWNT-Si junction was formed after transferring the self-assembled SWNT film onto an n-type Si wafer (doping level $\sim 10^{15}$ cm^{-3}) which has a 3 mm × 3

mm bare Si contact window in the center (Figure 3d). The current density–voltage (*J-V*) characteristics of the SWNT-Si solar cells fabricated with μ-HN, collapsed HN and porous HN were obtained under 100 mA/cm^2 AM 1.5G illumination (Newport Co.) and dark conditions, as shown in Figure 3e. The J_{sc}, V_{oc} and FF are listed in Table 1. The pristine μ-HN SWNT-Si solar cell exhibited the highest, stable FF of 72%, with an ideality factor of 1.71 over the 300 to 500 mV range (obtained from the slope of the quasi-linear part of the logarithmic scale J-V curve under dark condition). To our knowledge, this ideality factor is the lowest reported thus far (*i.e.*, closest to an ideal device).[32] The PCE value of 5.91% was obtained immediately after the fabrication, and it gradually increased to 6.04% after three weeks in ambient conditions (Figure 3e).

The FF represents the quality of a solar cell, and is one of the three parameters characterizing solar cell performance along with V_{oc} and J_{sc}. The significant improvement in FF and ideality factor over previously reported values[10-16] is attributed to the hierarchical μ-HN, which simultaneously enhances carrier separation, collection and transport. The dense, cross-linked SWNT walls in the μ-HN act as efficient conduction pathways, essentially serving as a micro-grid electrode to collect the charge carriers generated from the adjacent micro-honeycomb cells. The micro-grid configuration in the μ-HN significantly shortens the minimum carrier diffusion path, resulting in more efficient photocurrent collection. In the solar cells fabricated using collapsed HN and porous HN, the micro-grid configuration still exists, which leads to the quite high FFs.

The photocurrent generation mechanism of carbon nanotube/n-Si solar cells is still not yet clear. Originally it was regarded as a p-n heterojunction solar cells,[10,11,14] so SWNTs with larger band gap, such as (6,5) and (7,5) enriched SWNTs were used[13] with the aim of increasing the

built-in potential. However, as graphene[33] could also work instead of carbon nanotubes, and the current result with larger-diameter SWNTs (average diameter of 2 nm) shows a better performance than (6,5) and (7,5) enriched samples, it can be inferred that SWNT film serve as a hole collector in carbon nanotube-Si solar cells (see Supporting Information S4 for spectrum response and detailed analysis).
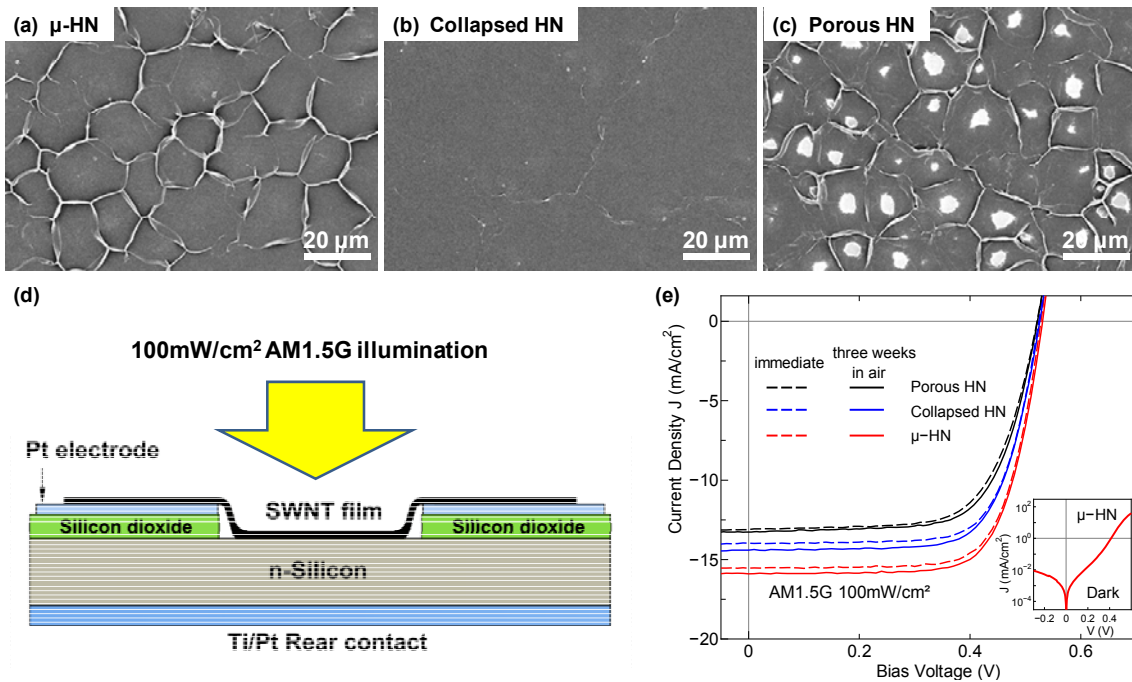

Figure 3. Three selected assemblies for the fabrication of solar cells and the photovoltaic performance of the fabricated solar cells. (a) μ-HN. (b) Collapsed HN. (c) Porous HN. (d) Schematic of SWNT-Si solar cell. (e) *J-V* characteristics of SWNT-Si solar cells with μ-HN, collapsed HN and porous HN measured under AM1.5 100mW/cm². The dashed line and solid line denote the *J-V* curve of the solar cells within three hours (immediate) and after three weeks after fabrication, respectively. The inset is the logarithmic scale *J-V* curve of μ-HN SWNT-Si solar cell under dark condition.

The samples with three aforementioned morphologies were all divided into halves, with one half of each used for solar cell fabrication and the other half transferred onto quartz substrates in order to characterize the electrical and optical properties of the self-assembled SWNT structures. The sheet resistance was measured by the four-point probe method (analyzer: Agilent 4156C; probe bed: Kyowa Riken K89PS), while optical transmittance spectra were obtained by UV-vis-

NIR spectroscopy (SHIMADZU UV-3150). As shown in Table 1, the sheet resistance of the μ-HN was 28.9% and 74.4% lower than those of the collapsed HN and the porous HN, respectively. The μ-HN also exhibited the highest transmittance over the AM1.5G spectrum ($T_{AM1.5G}$ = 35.0%). The substantial decrease in the sheet resistance and the increase in the transmittance are realized only by the morphology manipulation of SWNTs. Moreover, as part of the SWNT array aggregates into the wall structures, fewer SWNTs end up collapsed on the bottom of the cell, thereby blocking less light from reaching the Si surface. Hence, the μ-HN simultaneously shows higher transmittance and better conductivity than collapsed HN and porous HN structures.

Table 1. Optical transmittance and average sheet resistance of μ-HN, collapsed HN and porous HN, and the photovoltaic performance of the fabricated solar cells – FF, short-circuit current (J_{sc}) and open-circuit voltage (V_{oc}) – for SWNT-Si solar cells under AM1.5 and 100 mW/cm^2 illumination.

Within three hours of fabrication

self-assembled morphology	solar cell performance				film properties	
	PCE (%)	FF (%)	J_{sc} (mA/cm^2)	V_{oc} (mV)	R_{sh} (Ω/sq.)	$T_{AM1.5G}$ (%)
μ-HN	5.91	72	15.54	530	614	35.0
Collapsed HN	5.22	71	13.97	525	863	34.6
Porous HN	4.56	67	13.11	520	2397	28.1

After three weeks in air

self-assembled morphology	solar cell performance				film properties	
	PCE (%)	FF (%)	J_{sc} (mA/cm^2)	V_{oc} (mV)	R_{sh} (Ω/sq.)	$T_{AM1.5G}$ (%)
μ-HN	6.04	72	15.90	530	-	-
Collapsed HN	5.32	70	14.41	525	-	-
Porous HN	4.71	68	13.27	520	-	-

After nitric acid treatment

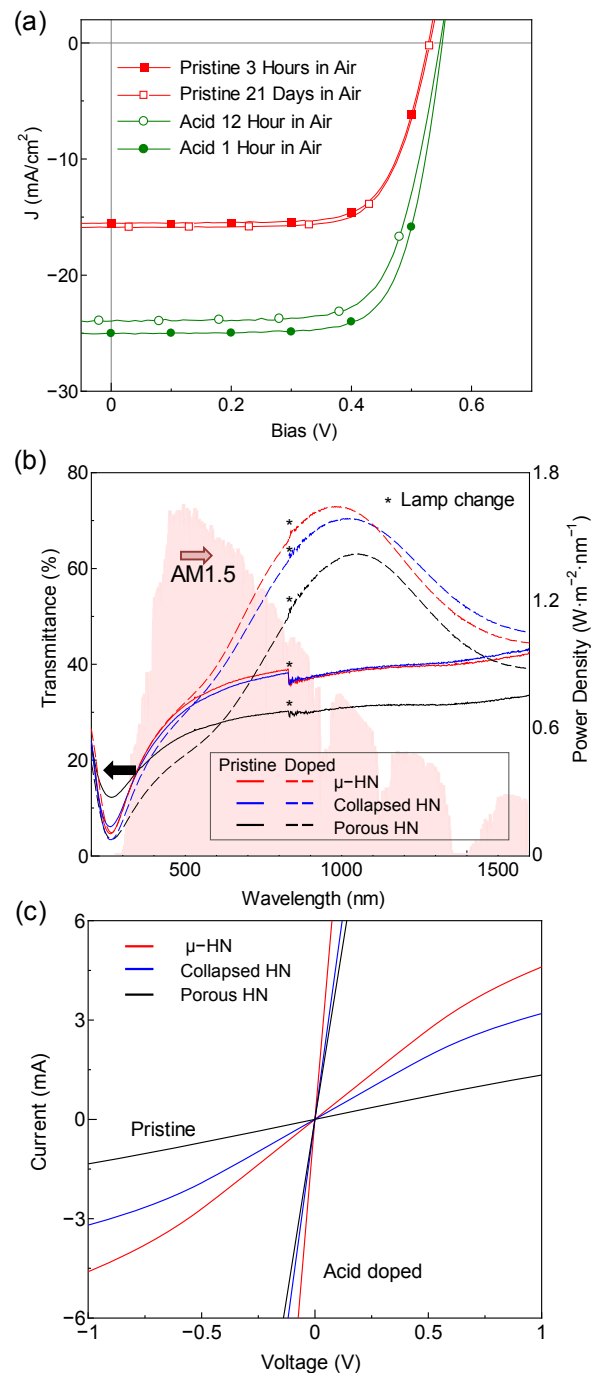| self-assembled morphology	solar cell performance				film properties	
	PCE (%)	FF (%)	J_{sc} (mA/cm^2)	V_{oc} (mV)	R_{sh} (Ω/sq.)	$T_{AM1.5G}$ (%)
μ-HN	10.02	73	25.01	550	105	48.5
Collapsed HN	8.35	73	20.68	550	120	46.3
Porous HN	8.30	69	21.86	550	139	37.0

Figure 4. (a) *J-V* characteristics of a micro-honeycomb structured SWNT-Si solar cell measured three hours and 21 days after device fabrication (shown in red), as well as 1 h and 12 h after dilute nitric acid doping (shown in green). (b) UV-vis-NIR transmittance spectra of μ-HN, collapsed HN and porous HN for pristine (solid) and doped (dashed) conditions (left ordinate) with AM1.5G power density spectrum (right ordinate). (c) Sheet resistance of μ-HN, collapsed HN and porous HN structures before and after acid doping.

10

A doping process was then carried out by dropping 120 μL of 2.4 M nitric acid onto the device which was heated to 50 ˚C using a hot plate. The μ-HN structure remains almost unchanged after the acid doping process (see Supporting Information S3). After drying, the PCE reached 10.02%, with an even higher FF of 73%. The *J-V* characteristics of the SWNT-Si solar cells after doping are shown in Figure 4a. The open-circuit voltage and short-circuit current after doping increased to 0.55V and 25.01 mA/cm^2, respectively. The PCE value of the μ-HN SWNT-Si solar cell decreased to 9.29% after 12 hours, which may be attributed to accelerated oxidation at the Si surface. The reduction of PCE after acid treatment has also been reported previously.[14-16] A substantial increase in the transmittance spectrum from 600 nm to 1200 nm (Figure 4b) and a five-fold decrease in the sheet resistance (from 614 Ω/sq. to 105 Ω/sq., as shown in Figure 4c) contribute to the increase of the PCE. The doping of the film also helps increase the charge collection efficiency. The dramatic changes in the electrical and the optical properties result from charge transfer from the SWNTs[34] induced by the nitric acid. Depletion of electrons from the valence band results in a shift in the Fermi level and the attenuation of absorption peaks. The decrease of sheet resistance may be also attributed to further bundling of SWNTs. A detailed comparison of morphology and Raman spectra is discussed in the Supporting Information S3.

In summary, we propose a simple water vapor treatment to engineer the structure of VA-SWNTs into a micro-honeycomb network. The hierarchical μ-HN consists of dense walls and a buckypaper bottom, which simultaneously increases the optical transmittance and decreases the sheet resistance. Applying μ-HN to the SWNT-Si solar cell results in both high PCE and high FF. Note that the achieved PCE is obtained with only 35.0% transparency and without any efforts made to optimize the SWNT chirality, diameter or length. We believe the hierarchical μ-HN is very promising for applications of SWNT-Si solar cells.

Experimental Methods

Synthesis of High-Purity SWNT by ACCVD. VA-SWNTs were synthesized by the standard alcohol-catalytic CVD (ACCVD) method with Co/Mo dip-coated on Si/SiO$_2$ substrates. The substrate loaded with Co/Mo bimetallic nanoparticle catalysts was placed in a quartz tube surrounded by the electric furnace after the dip-coating process and heated under a flow of 300 sccm of Ar containing 3% H$_2$ at 40 kPa to 800 ˚C in 30 min. The substrate was then kept at 800 ˚C for 10 min before ethanol feedstock (dehydrated, 99.5%, Wako Chemical, Inc.) was introduced with a flow rate of 100 sccm at 1.3 kPa. The growth process of VA-SWNTs can be monitored by the *in situ* laser absorption technique for quartz substrates.[35]

Fabrication of SWNT-Si Solar Cell. The n-type Si substrate (CZ growth, <100>axis, 7.5-12.5 Ω·cm, 100 nm SiO$_2$, Lot# 1-41072-000, SUMCO Co.) was treated by 5 M NaOH (Wako Co., Ltd.) at 90 ˚C for 30 min to remove the oxide layer, followed by rinsing in RCA2 solution (V_{H_2O}:V_{HCl}:$V_{H_2O_2}$= 5:1:1). The 3 mm by 3 mm bare Si contact window was surrounded by a 200-nm-thick SiO$_2$ as the insulating layer and a 100-nm-thick Pt electrode by sputtering (ULVAC-RIKO, Inc.). 10-nm-thick Ti and 50-nm-thick Pt layers were subsequently sputtered onto the back of the Si substrate as the rear contact. The SWNT films were transferred onto the substrate by a hot-water thermocapillary process[31] and dried in ambient environment.

Supporting Information Available: Raman spectroscopy of SWNTs before and after water vapor treatment, discussion on the formation of micro-honeycomb structure and the effect of acid doping on the morphology and Raman spectrum and discussion on the wavelength dependence of photocurrent generation. This material is available free of charge via the Internet at http://pubs.acs.org.

REFERENCES

(1)   Avouris, P.; Freitag, M.; Perebeinos, V. Carbon-Nanotube Photonics and Optoelectronics. *Nat. Photonics* **2008,** *2*, 341−350.

(2)   De Volder, M. F. L.; Tawfick, S. H.; Baughman, R. H.; Hart, A. J. Carbon Nanotubes: Present and Future Commercial Applications. *Science* **2013,** *339*, 535−539.

(3)   Guldi, D. M.; Costa, R. D. Nanocarbon Hybrids: The Paradigm of Nanoscale Self-Ordering/Self-Assembling by Means of Charge Transfer/Doping Interactions. *J. Phys. Chem. Lett.* **2013**, *4*, 1489-1501.

(4)   Bindl, D. J.; Wu, M. −Y.; Prehn, F. C.; Arnold, M. S. Efficiently Harvesting Excitons from Electronic Type-Controlled Semiconducting Carbon Nanotube Films. *Nano Lett.* **2011**, *11*, 455-460.

(5)   Jain, R. M.; Howden, R.; Tvrdy, K.; Shimizu, S.; Hilmer, A. J.; McNicholas, T. P.; Gleason, K. K.; Strano, M. S. Polymer-Free Near-Infrared Photovoltaics with Single Chirality (6,5) Semiconducting Carbon Nanotube Active Layers. *Adv. Mater*. **2012**, *24*, 4436-4439.

(6)   Brown, P.; Takechi, K.; Kamat, P. Single-Walled Carbon Nanotube Scaffolds for Dye-Sensitized Solar Cells. *J. Phys. Chem. C* **2008**, *112*, 4776-4782.

(7)   Dang, X. N.; Yi, H.; Ham, M. –H.; Qi, J.; Dong, S. Y.; Ladewski, R.; Strano, M. S.; Hammond, P. T.; Belcher, A. M. Virus-Templated Self-Assembled Single-Walled Carbon Nanotubes for Highly Efficient Electron Collection in Photovoltaic Devices. *Nat. Nanotechnol*. **2011**, *6*, 377-384.

(8)   Aitola, K.; Kaskela, A.; Halme, J.; Ruiz, V.; Nasibulin, A. G.; Kauppinen, E. I.; Lund, P. Single-Walled Carbon Nanotube Thin-Film Counter Electrodes for Indium Tin Oxide-Free Plastic Dye Solar Cells. *J. Electrochem. Soc*. **2010**. *12*, B1831-B1837.

(9)   Hao, F.; Dong, P.; Zhang, Y.; Loya, P. E.; Hauge, R. H.; Li, J.; Lou, J.; Lin, H. High Electrocatalytic Activity of Vertically Aligned Single-Walled Carbon Nanotubes towards Sulfide Redox Shuttles. *Sci. Rep*. **2012**, *2*, 368.

(10)   Wei, J.; Jia, Y.; Shu, Q.; Gu, Z.; Wang, K.; Zhuang, D.; Zhang, G.; Wang, Z.; Luo, J.; Cao, A.; et al. Double-Walled Carbon Nanotube Solar Cells. *Nano Lett*. **2007,** *7*, 2317–2321.

(11)   Jia, Y.; Wei, J.; Wang, K.; Cao, A.; Shu, Q.; Gui, X.; Zhu, Y.; Zhuang, D.; Zhang, G.; Ma, B.; et al. Nanotube–Silicon Heterojunction Solar Cells. *Adv. Mater*. **2008,** *20*, 4594–4598.

(12)   Wadhwa, P.; Liu, B.; McCarthy, M. A.; Wu, Z.; Rinzler, A. G. Electronic Junction Control in a Nanotube-Semiconductor Schottky Junction Solar Cell. *Nano Lett.* **2010,** *10*, 5001–5005.

(13)   Kozawa, D.; Hiraoka, K.; Miyauchi, Y.; Mouri, S.; Matsuda, K. Analysis of the Photovoltaic Properties of Single-Walled Carbon Nanotube/Silicon Heterojunction Solar Cells. *Appl. Phys. Exp.* **2012,** *5*, 042304.

(14)   Jia, Y.; Cao, A.; Bai, X.; Li, Z.; Zhang, L.; Guo, N.; Wei, J.; Wang, K.; Zhu, H.; Wu, D.; et al. Achieving High Efficiency Silicon-Carbon Nanotube Heterojunction Solar Cells by Acid Doping. *Nano Lett.* **2011,** *11*, 1901–1905.

(15)   Jung, Y.; Li, X.; Rajan, N. K.; Taylor, A. D.; Reed, M. A. Record High Efficiency Single-Walled Carbon Nanotube/Silicon p–n Junction Solar Cells. *Nano Lett.* **2012,** *13*, 95–99.

(16)   Shi, E.; Zhang, L.; Li, Z.; Li, P.; Shang, Y.; Jia, Y.; Wei, J.; Wang, K.; Zhu, H.; Wu, D.; et al. TiO_2-Coated Carbon Nanotube-Silicon Solar Cells with Efficiency of 15%. *Sci. Rep.* **2012,** *2*, 884.

(17)   Svrcek, V.; Cook, S.; Kazaoui, S.; Kondo, M. Silicon Nanocrystals and Semiconducting Single-Walled Carbon Nanotubes Applied to Photovoltaic Cells. *J. Phys. Chem. Lett.* **2011**, *2*, 1646-1650.

(18)   Duan, H.; Berggren, K. K. Directed Self-Assembly at the 10 nm Scale by Using Capillary Force-Induced Nanocohesion. *Nano Lett.* **2010,** *10*, 3710-3716.

(19)   Pokroy, B.; Kang, S. H.; Mahadevan, L.; Aizenberg, J. Self-Organization of a Mesoscale Bristle into Ordered, Hierarchical Helical Assemblies. *Science* **2009,** *323*, 237-240.

(20)   Liu, H.; Li, S.; Zhai, J.; Li, H.; Zheng, Q.; Jiang, L.; Zhu, D. Self-Assembly of Large-Scale Micropatterns on Aligned Carbon Nanotube Films. *Angew. Chem., Int. Ed.* **2004,** *43*, 1146-1149.

(21)   Chakrapani, N.; Wei, B.; Carrillo, A.; Ajayan, P. M.; Kane, R. S. Capillarity-Driven Assembly of Two-Dimensional Cellular Carbon Nanotube Foams. *Proc. Natl. Acad. Sci. USA* **2004,** 101, 4009-4012.

(22)   De Volder, M.; Tawfick, S. H.; Park, S. J.; Copic, D.; Zhao, Z.; Lu, W.; Hart, A. J. Diverse 3D Microarchitectures Made by Capillary Forming of Carbon Nanotubes. *Adv. Mater.* **2010,** *22*, 4384-4389.

(23)   Lim, X.; Foo, H. W. G.; Chia, G. H.; Sow, C.-H. Capillarity-Assisted Assembly of Carbon Nanotube Microstructures with Organized Initiations. *ACS Nano* **2010,** *4*, 1067-1075.

(24)   De Volder, M.; Hart, A. J. Engineering Hierarchical Nanostructures by Elastocapillary Self-Assembly. *Angew. Chem., Int. Ed.* **2013,** *52*, 2412-2425.

(25)   Futaba, D. N.; Hata, K.; Yamada, T.; Hiraoka, T.; Hayamizu, Y.; Kakudate, Y.; Tanaike, O.; Hatori, H.; Yumura, M.; Iijima, S. Shape-Engineerable and Highly Densely Packed Single-Walled Carbon Nanotubes and Their Application as Super-Capacitor Electrodes. *Nat. Mater.* **2006,** *5*, 987–994.

(26)   Wakamatsu, N.; Takamori, H.; Fujigaya, T.; Nakashima, N. Self-Organized Single-Walled Carbon Nanotube Conducting Thin Films with Honeycomb Structures on Flexible Plastic Films. *Adv. Func. Mater.* **2009,** *19*, 311–316.

(27)   Takamori, H.; Fujigaya, T.; Yamaguchi, Y.; Nakashima, N. Simple Preparation of Self-Organized Single-Walled Carbon Nanotubes with Honeycomb Structures. *Adv. Mater.* **2007,** *19*, 2535–2539.

(28)   Wu, Z.; Chen, Z.; Du, X.; Logan, J. M.; Sippel, J.; Nikolou, M.; Kamaras, K.; Reynolds, J. R.; Tanner, D. B.; Hebard, A. F.; et al. Transparent, Conductive Carbon Nanotube Films. *Science* **2004,** *305*, 1273–1276.

(29)   Maruyama, S.; Kojima, R.; Miyauchi, Y.; Chiashi, S.; Kohno, M. Low-Temperature Synthesis of High-Purity Single-Walled Carbon Nanotubes from Alcohol. *Chem. Phys. Lett.* **2002,** *360*, 229–234.

(30)   Murakami, Y.; Chiashi, S.; Miyauchi, Y.; Hu, M.; Ogura, M.; Okubo, T.; Maruyama, S. Growth of Vertically Aligned Single-Walled Carbon Nanotube Films on Quartz Substrates and Their Optical Anisotropy. *Chem. Phys. Lett.* **2004,** *385*, 298–303.

(31)   Murakami, Y.; Maruyama, S. Detachment of Vertically Aligned Single-Walled Carbon Nanotube Films from Substrates and Their Re-attachment to Arbitrary Surfaces. *Chem. Phys. Lett.* **2006,** *422*, 575–580.

(32)   Tune, D. D.; Flavel, B. S.; Krupke, R.; Shapter, J. G. Carbon Nanotube-Silicon Solar Cells. *Adv. Energy Mat.* **2012,** *2*, 1043–1055.

(33)   Miao, X.; Tongay, S.; Petterson, M. K.; Berke, K.; Rinzler, A. G.; Appleton, B. R.; Hebard, A. F. High Efficiency Graphene Solar Cells by Chemical Doping. *Nano Lett.* **2012**, *12*, 2745-2750

(34)   Zhou, W.; Vavro, J.; Nemes N. M.; Fischer, J. E.; Borondics, F.; Kamarás, K.; Tanner, D. B. Charge Transfer and Fermi Level Shift in p-doped Single-Walled Carbon Nanotubes. *Phys. Rev. B* **2005**, *71*, 205423.

(35)   Maruyama, S.; Einarsson, E.; Murakami, Y.; Edamura, T. Growth Process of Vertically Aligned Single-Walled Carbon Nanotubes. *Chem. Phys. Lett.* **2005,** *403*, 320–323.

Supporting Information

Self-Assembled Micro-Honeycomb Network of

Single-Walled Carbon Nanotubes for Solar Cells

Kehang Cui,[1] Takaaki Chiba,[1] Shuichiro Omiya,[1] Theerapol Thurakitseree,[1] Pei Zhao,[1]

Shunjiro Fujii,[2] Hiromichi Kataura,[2] Erik Einarsson,[1] Shohei Chiashi,[1] Shigeo Maruyama[1]*

[1] Department of Mechanical Engineering, The University of Tokyo, 7-3-1 Hongo, Bunkyo-ku, Tokyo 113-8656, Japan

[2] Nanosystem Research Institute, National Institute of Advanced Industrial Science and Technology, 1-1-1 Higashi, Tsukuba 305-8562, Japan

S1. Raman spectroscopy of as-synthesized and μ-HN of SWNTs
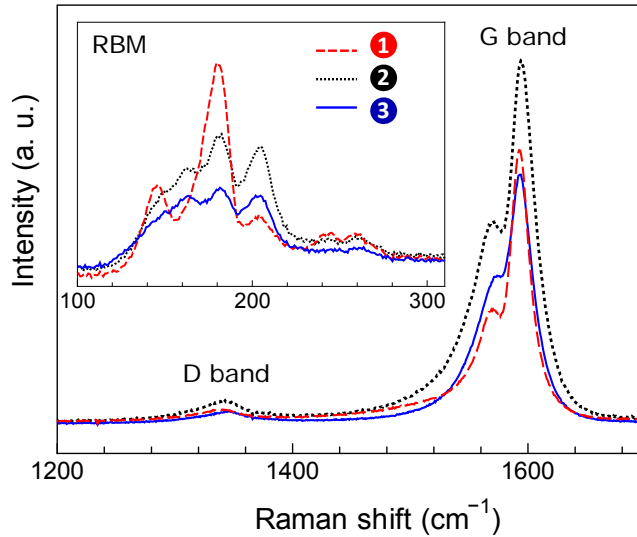
Figure S1. Resonance Raman spectra of SWNTs before and after water vapor treatment: spectrum 1 corresponds to as-synthesized VA-SWNTs. Spectra 2 and 3 correspond to the wall and bottom of the micro-honeycomb structure, respectively. All spectra were measured with a 488 nm excitation laser incident normal to the substrate.

Raman spectra were measured to characterize and compare the SWNT assemblies before and after water vapor treatment. Spectrum 1 in Figure S1 corresponds to as-synthesized VA-SWNTs, whereas spectra 2 and 3 were obtained from the highly condensed walls and buckypaper bottom, respectively. Spectrum 1 shows that the D-band is negligible for the as-synthesized VA-SWNTs, indicating the high quality and high purity of as-synthesized VA-SWNTs. Furthermore, the relative D-band intensity was nearly unchanged after water vapor treatment. This illustrates that the water vapor treatment did not induce defects in SWNTs. In the radial breathing mode (RBM) region (the inset of Figure S1), spectrum 1 has the characteristic of free-standing SWNTs, with strong peaks appearing at 181 cm^{-1}.[S1] The two characteristic peaks became much weaker after the water vapor treatment (spectra 2 and 3), owing to the morphology change of SWNTs. The reduction in peak intensity was more pronounced in the bottom of the honeycomb cell.

S2. Discussion on the μ-HN formation

The water reservoir temperature and the vapor exposure time are the two dominant factors determining the μ-HN formation. As the control, a 10 μL water droplet was dropped onto the top surface of a VA-SWNT film at room temperature. After evaporation of the water, the SWNTs had aggregated into a highly condensed bulk and generated many 100 μm-scale gaps (Figures S2-1a and S2-1b), which is in agreement with the report by Futaba *et al.* [S2] A similar phenomenon was observed for an ethanol droplet and an 80 ˚C water droplet. In the case of water vapor treatment, when the water reservoir temperature was increased to 50 ˚C, the length of the gaps decreased to ~50 μm and honeycomb cells started to form (Figure S2-2a). Further increase of the water reservoir temperature to 70 ˚C significantly reduced the size of the gaps to approximately 5 μm, and the size of honeycomb cells became more uniform (Figure S2-2b). A well-formed μ-HN was obtained when the water reservoir temperature reached 80 ˚C (Figure S2-2c). The vapor exposure time for the structures shown in Figures S2-2a, S2-2b and S2-3c was 5 s in all cases.

The effect of vapor exposure time on the morphology was investigated using a constant water reservoir temperature of 80 ˚C. Extending the exposure time from 2 s to 5 s resulted in an increase in micro-honeycomb cell size from ~2.5 μm (Figure S2-3a) to ~12 μm (Figure S2-3b). When the exposure time was longer than 15 s, the walls of the cells nearly disappeared, as most of the VA-SWNTs had collapsed as shown in Figure S2-3c. Compared with direct immersion or direct wetting (water droplet) [S3], water vapor treatment is a more delicate, controllable method.
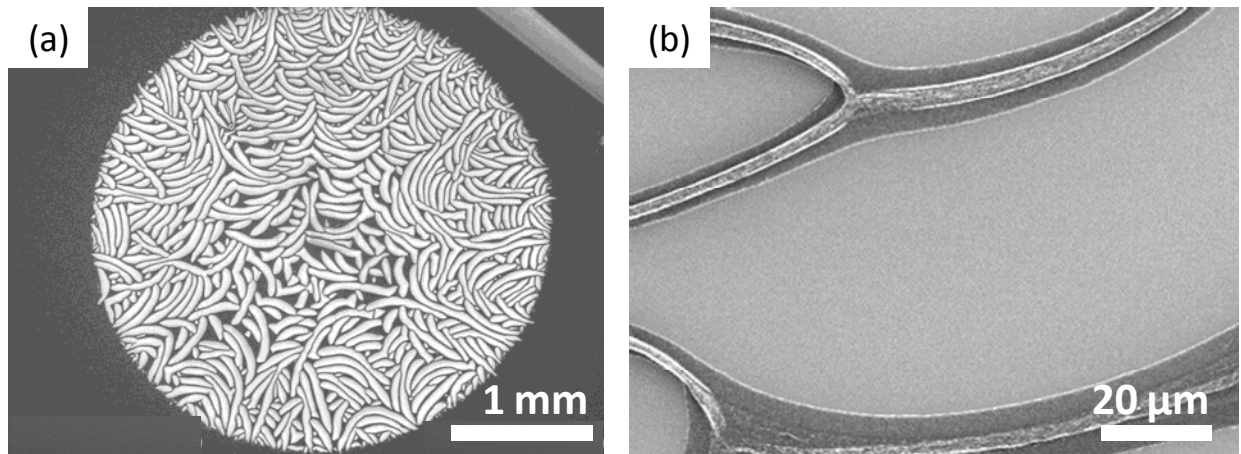
Figure S2-1. 100 μm-scale gaps obtained by applying a 10 μL water droplet to the surface at RT under (a) low magnification and (b) high magnification.
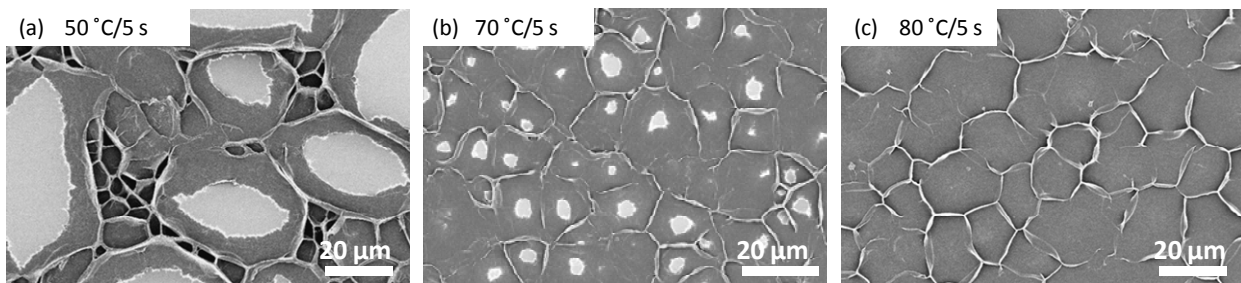

Figure S2-2. (a-c) Morphologies obtained by exposure to 50 ºC, 70 ºC and 80 ºC water reservoirs, respectively. The vapor exposure time for each vapor treatment step is 5 s.
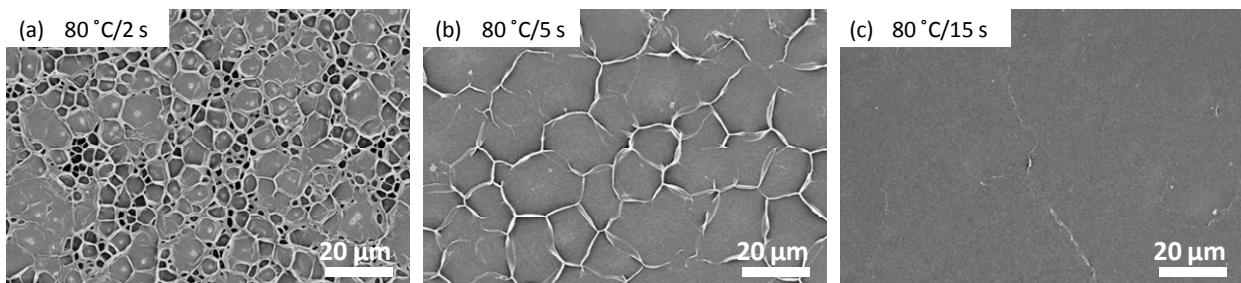

Figure S2-3. (a-c) Morphologies obtained with vapor exposure times of 2 s, 5 s and 15 s for each iteration, respectively. Reservoir temperature was 80 ºC.

S3. Effect of nitric acid treatment on the properties of μ-HN

To investigate the effect of nitric acid treatment on the morphology of μ-HN, we observed the SEM images, as shown in Figures S3-1a and S3-1b. The micro-honeycomb structure did not change as a whole, but the top of the walls appeared slightly compressed. The Raman spectra in Figure S3-2 show a 21 cm^{-1} upshift in both the G band and the G′ band as well as a significant increase in D band intensity. The Raman spectra further prove that the SWNTs samples are heavily p-doped[S4].
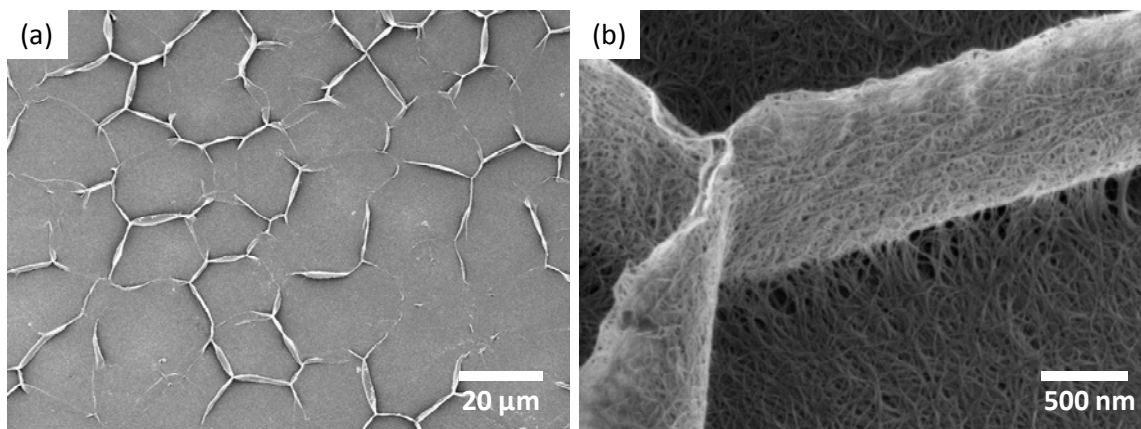

Figure S3-1. SEM images the μ-HN after acid doping. (a) Long-range morphology. (b) Magnified image of the wall in the μ-HN.
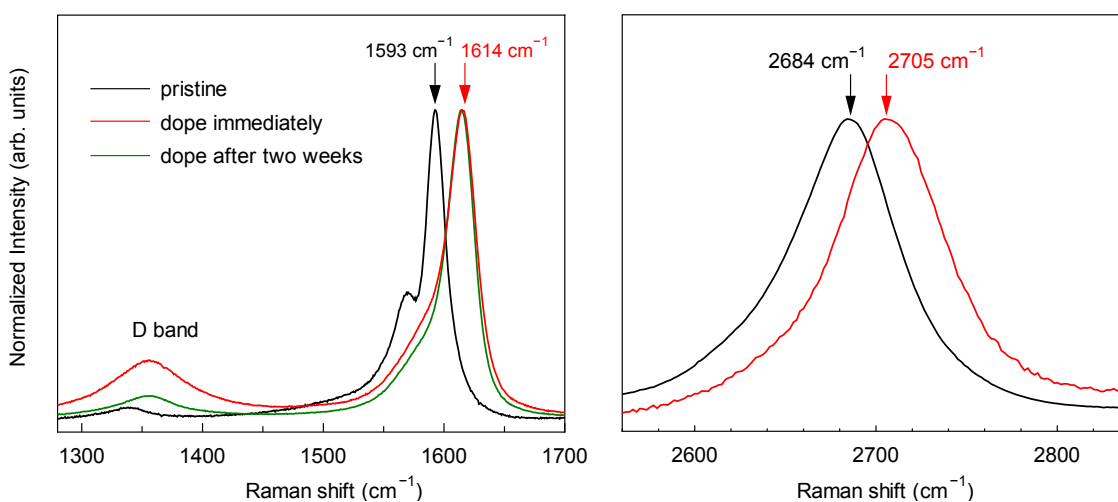

Figure S3-2. Raman spectra of pristine and nitric acid treated samples. Spectra of the treated samples were measured immediately after the samples were completely dried.

S4. Wavelength dependence of photocurrent generation

   The spectrum responses (SM-250TF, Bunkoukeiki Co. Ltd) of both SWNT-Si solar cell and Si

p-n junction solar cell (Si photodiode S1337, Hamamatsu Photonics K.K.) were obtained to

discuss the wavelength dependence of the photocurrent generation. As shown in Figure S4, there

is almost no external quantum efficiency when the photon energy is smaller than the silicon band

gap (~1100 nm) for the SWNT-Si solar cell. Moreover, the SWNT-Si solar cell showed a similar

shape as the conventional Si *p-n* junction solar cell. No obvious correlation between the SWNT

absorption and the SWNT-Si spectrum response was observed in the 300 nm ~ 1150 nm range.

This may be attributed to that the diameter of the SWNTs used in this research is around 2 nm,

so that the main absorption peak E_{11} is around 2400 nm wavelength in the infrared region. This

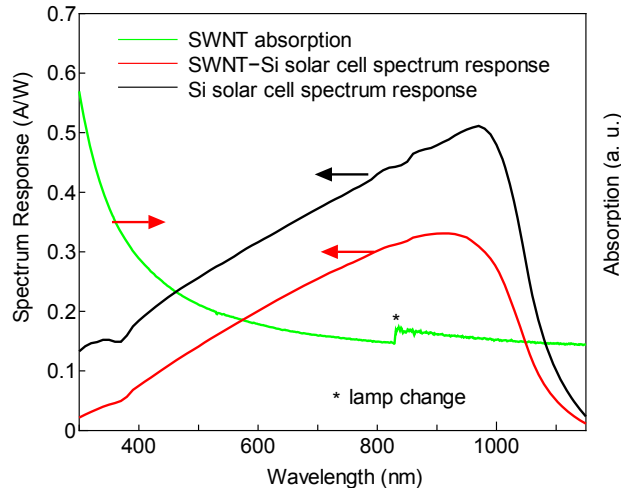result further supports that the SWNT-Si solar cell is inversion type solar cell.

Figure S4. External quantum efficiency of the SWNT-Si solar cell and Si solar cell (left y axis), as well as the absorption spectrum of the SWNT therein (right y axis).

Reference

S1. Zhang, Z.; Einarsson, E.; Murakami, Y.; Miyauchi, Y.; Maruyama, S. Polarization Dependence of Radial Breathing Mode Peaks in Resonant Raman Spectra of Vertically Aligned single-Walled Carbon Nanotubes. *Phys. Rev. B* **2010**, *81*, 165442.

S2. Futaba, D. N.; Hata, K.; Yamada, T.; Hiraoka, T.; Hayamizu, Y.; Kakudate, Y.; Tanaike, O.; Hatori, H.; Yumura, M.; Iijima, S. Shape-Engineerable and Highly Densely Packed Single-Walled Carbon Nanotubes and Their Application as Super-Capacitor Electrodes. *Nat. Mater.* **2006,** *5*, 987-994.

S3. De Volder, M.; Hart, A. J. Engineering Hierarchical Nanostructures by Elastocapillary Self-Assembly. *Angew. Chem., Int. Ed.* **2013**, *52*, 2412-2425.

S4. Zhou, W.; Vavro, J.; Nemes N. M.; Fischer, J. E.; Borondics, F.; Kamarás, K.; Tanner, D. B. Charge Transfer and Fermi Level Shift in p-doped Single-Walled Carbon Nanotubes. *Phys. Rev. B* **2005**, *71*, 205423